AD

STRESS-CORROSION CRACKING OF
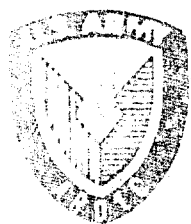# LIQUID-PHASE SINTERED TUNGSTEN ALLOYS

M. Z. SHAH KHAN

J. H. UNDERWOOD

I. A. BURCH

DTIC
ELECTE
DEC 2 1 1988
D

OCTOBER 1988

US ARMY ARMAMENT RESEARCH,
DEVELOPMENT AND ENGINEERING CENTER
CLOSE COMBAT ARMAMENTS CENTER
BENÉT LABORATORIES
WATERVLIET, N.Y. 12189-4050

BENÉT LABS

APPROVED FOR PUBLIC RELEASE; DISTRIBUTION UNLIMITED

88 12 21 056

DISCLAIMER

The findings in this report are not to be construed as an official Department of the Army position unless so designated by other authorized documents.

The use of trade name(s) and/or manufacturer(s) does not constitute an official indorsement or approval.

DESTRUCTION NOTICE

For classified documents, follow the procedures in DoD 5200.22-M, Industrial Security Manual, Section II-19 or DoD 5200.1-R, Information Security Program Regulation, Chapter IX.

For unclassified, limited documents, destroy by any method that will prevent disclosure of contents or reconstruction of the document.

For unclassified, unlimited documents, destroy when the report is no longer needed. Do not return it to the originator.

ADA203201

REPORT DOCUMENTATION PAGE	READ INSTRUCTIONS BEFORE COMPLETING FORM

1. REPORT NUMBER	2. GOVT ACCESSION NO.	3. RECIPIENT'S CATALOG NUMBER
ARCCB-TR-88039		

4. TITLE (and Subtitle)	5. TYPE OF REPORT & PERIOD COVERED
STRESS-CORROSION CRACKING OF LIQUID-PHASE SINTERED TUNGSTEN ALLOYS	Final
	6. PERFORMING ORG. REPORT NUMBER

7. AUTHOR(s)	8. CONTRACT OR GRANT NUMBER(s)
M. Z. Shah Khan, J. H. Underwood, and I. A. Burch (See Reverse)	

9. PERFORMING ORGANIZATION NAME AND ADDRESS	10. PROGRAM ELEMENT, PROJECT, TASK AREA & WORK UNIT NUMBERS
US Army ARDEC Benet Laboratories, SMCAR-CCB-TL Watervliet, NY 12189-4050	AMCMS No. 6126.23.1BL0.0 PRON No. 1A82ZJWLNMSC

11. CONTROLLING OFFICE NAME AND ADDRESS	12. REPORT DATE
US Army ARDEC Close Combat Armaments Center Picatinny Arsenal, NJ 07806-5000	October 1988
	13. NUMBER OF PAGES
	28

14. MONITORING AGENCY NAME & ADDRESS(if different from Controlling Office)	15. SECURITY CLASS. (of this report)
	UNCLASSIFIED
	15a. DECLASSIFICATION/DOWNGRADING SCHEDULE

16. DISTRIBUTION STATEMENT (of this Report)

Approved for public release; distribution unlimited.

17. DISTRIBUTION STATEMENT (of the abstract entered in Block 20, if different from Report)

18. SUPPLEMENTARY NOTES

To be presented at the Seventh International Conference on Fracture, University of Houston, Houston, TX, March 1989.
Accepted for publication in Proceedings of the Conference.

19. KEY WORDS (Continue on reverse side if necessary and identify by block number)

Stress-Corrosion Cracking	Kinetic Energy Penetration
Liquid-Phase Tungsten	Fracture Mechanics
Unloading Compliance	Crack Closure

20. ABSTRACT (Continue on reverse side if necessary and identify by block number)

This study addresses the stress-corrosion cracking susceptibility of liquid-phase sintered tungsten alloys during long-term storage. These alloys are used for kinetic energy penetrators in military applications and it is essential that the structural integrity of the penetrator is not diminished due to the combined action of the chemical environment and the residual manufacturing stresses.

(CONT'D ON REVERSE)

7. AUTHORS (CONT'D)

M. Z. Shah Khan and I. A. Burch
Materials Research Laboratories
Defence Science and Technology Organisation
P.O. Box 50
Ascot Vale, Victoria, 3032
Australia

20. ABSTRACT (CONT'D)

This report describes test methods used for assessing the resistance to stress-corrosion cracking in terms of the stress intensity parameter, K_{Iscc}. The alloys were obtained from different sources and had up to 10 weight percent additions of selected combinations of nickel (Ni), iron (Fe), copper (Cu), and cobalt (Co), and different process variables. Cantilever-bend specimens were used and the test environment was an immersion in 3.5 percent sodium chloride (NaCl) aqueous solution followed by sustained loading in 95 percent relative humidity air.

The findings of this study were as follows: (1) Fracture mechanics was shown to give a good assessment and ranking of the resistance to stress-corrosion cracking of the various alloys. (2) Evidence of stress-corrosion cracking was found in the region controlled by the stress intensity factor, generally designated as region III. (3) An unloading compliance procedure similar to that applied in J-integral testing was shown to give accurate measurements of stress-corrosion crack growth. (4) A crack closure phenomenon was identified using the unloading compliance procedure and attributed to the accumulation of corrosion products between the crack faces following certain exposure times to the environment.

Accesion For

NTIS CRA&I	☑
DTIC TAB	☐
Unannounced	☐
Justification	

By

Distribution

Availability Codes

Dist | Avail and/or Special

A-1

QUALITY INSPECTED 2

TABLE OF CONTENTS

TABLES

LIST OF ILLUSTRATIONS

ACKNOWLEDGEMENTS

INTRODUCTION

Liquid-phase sintered tungsten alloys are produced by a powder metallurgical technique in which powders of tungsten (W), nickel (Ni), iron (Fe), and copper (Cu) are compacted and then sintered at about 1400°C in a dry hydrogen atmosphere. The resulting alloys possess high strength and density, and their typical microstructure consists of rounded hard tungsten particles surrounded by a comparatively soft matrix phase (or binder) rich in the above elements.

Previous work was directed toward improving the strength and ductility of sintered tungsten alloys by controlling their composition (refs 1,2) and processing (refs 3-7), such as rate of cooling from the sintering temperature. The stress-corrosion cracking susceptibility of high density liquid-phase sintered tungsten alloys has not been investigated extensively. In a recent study, Chung and Duquette (ref 8) investigated two tungsten alloys. In general, their study showed that a 90W-7Fe-3Ni alloy was susceptible to stress-corrosion cracking in a sodium chloride (NaCl) solution, while a 97WNiFeCuCo alloy was immune to such cracking after 200 hours of exposure. The current investigation addresses the stress-corrosion cracking susceptibility of sintered tungsten alloy systems during long-term storage. These alloys are used as long rod kinetic energy penetrators in military applications. It is essential that both the launch integrity and target-penetration capability of the penetrator are not diminished due to the combined action of sustained loading and chemical environment. Residual manufacturing stresses may be present in the penetrators, and exposure to a saline environment is common during storage of naval munitions.

Four alloys of various tungsten and binder composition were studied to determine their threshold stress intensities for stress-corrosion cracking

_____

References are listed at the end of this report.

1

(K_{Iscc}) by applying a fracture mechanics analysis. In addition to the determination of K_{Iscc} values, an unloading compliance procedure was applied to measure crack growth under environmental conditions. The advantages of using the compliance procedure and the results are discussed in the following sections. Using tensile test and indentation hardness data for one alloy system, a hardness-strength correlation was determined and was utilized to estimate the ultimate tensile strength of the other three alloy systems. Detailed microprobe analyses were performed to obtain the chemical composition of the binder phase in each alloy system. The fracture surfaces were studied using scanning electron microscopy (SEM) and the stress-corrosion fracture mechanisms are described.

MATERIALS

Four tungsten-based alloys were selected for this study: 95WNiFe, 97WNiFeCuCo, 90WFeNi, and 90WNiCu. Table I lists the nominal alloy compositions and the average compositions of the binder phase obtained from electron microprobe analyses. Microstructures of the alloys studied are shown in Figure 1. Note that the tungsten particle size is clearly the largest in alloy 97WNiFeCuCo. The 90WNiCu alloy contained two binder phases as shown in Table I.

All tests on the above alloys were performed in the as-received condition. The post-sintering treatment for alloy 95WNiFe consisted of vacuum annealing at 1100°C followed by rapid air cooling. Alloys 97WNiFeCuCo and 90WNiCu were in the as-sintered condition. The post-sintering treatment for alloy 90WFeNi was vacuum annealing at 1050°C for 1 hour, water quenching, followed by a swaging operation of approximately 24 percent area reduction. Following swaging, alloy 90WFeNi was subjected to a heat treatment at 550°C for 1 hour, and then air cooled.
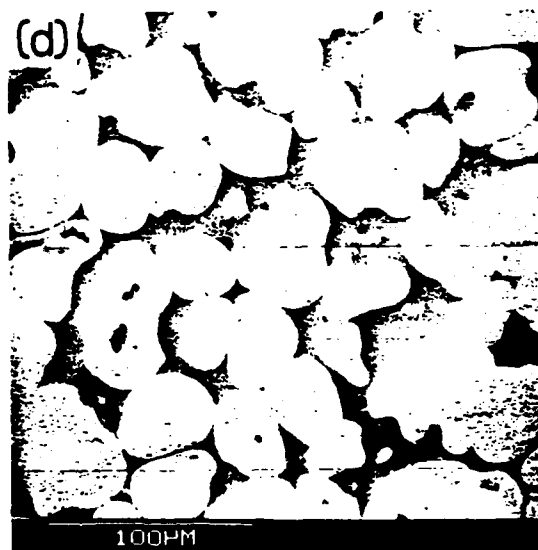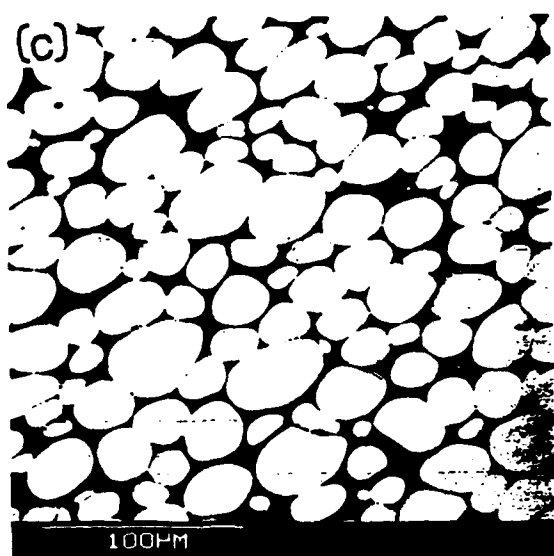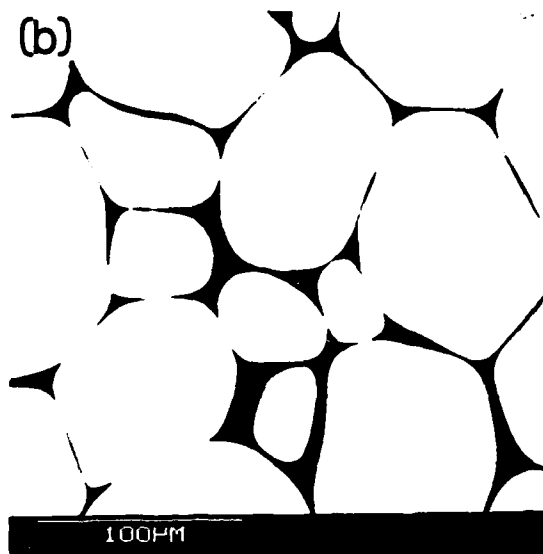
2
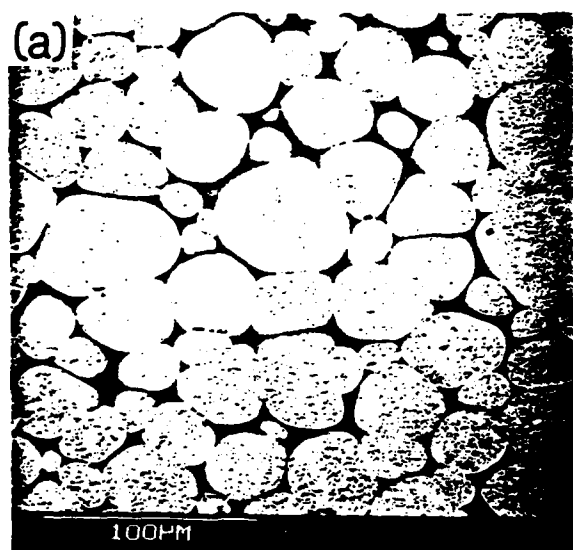
Figure 1. Microstructure of the alloys investigated: (a) 95WNiFe,
(b) 97WNiFeCuCo, (c) 90WFeNi, and (d) 90WNiCu. SEM
photos of polished surfaces etched with Murakami's reagent.

TABLE I. MATERIAL COMPOSITION, WEIGHT PERCENT

Alloy		W	Fe	Ni	Cu	Co
90WFeNi	Nominal	90.0	5.0	5.0	-	-
	Matrix Phase	23.0	38.3	38.7	-	-
90WNiCu	Nominal	90.0	-	7.5	2.5	-
	Matrix Phase-I	33.7	-	53.8	12.5	-
	Matrix Phase-II	2.4	-	38.4	59.3	-
97WNiFeCuCo	Nominal	97.0	0.7	1.6	0.5	0.1
	Matrix Phase	13.8	19.0	47.6	16.3	3.3
95WNiFe	Nominal	95.0	1.5	3.5	-	-
	Matrix Phase	26.2	21.0	52.5	-	-

Table II lists the hardness and density for the alloys in the as-received condition. Also included are the ultimate tensile strength and fracture toughness of the alloys; the procedures followed are described in the following sections.

TABLE II. PROPERTIES OF THE ALLOYS INVESTIGATED

Alloy	Brinell Hardness Number BHN	Density g/cm³	Ultimate Tensile Strength, MPa	Fracture Toughness MPa m$^{\frac{1}{2}}$
95WNiFe	283	18.1	901*	59.5***
97WNiFeCuCo	285	18.5	908**	49.5***
90WFeNi	395	16.9	1258**	54.5***
90WNiCu	290	17.1	924**	64.0***

*Determined from room temperature tensile tests.
**Determined using hardness/strength correlation.
***Determined by averaging K_{max} values obtained from three-point bend and cantilever-bend tests; only the toughness value for alloy 90WFeNi meets the ASTM requirements (ref 9).

4

EXPERIMENTAL METHODS

Cantilever-bend specimens were electric-discharge machined to the con-
figurations shown in Figure 2. Fatigue precracking was performed in three-point
bending with a cyclic frequency of 15 Hz using an MTS servo-hydraulic machine.
As recommended by ASTM Standard E-399 (ref 9), the maximum stress intensity was
kept below 60 percent of the K_{IC} value in the final 2.5 percent portion of the
crack length. The depth of the fatigue crack from the machined notch gave a
final a/W ratio of approximately 0.5. All precracking was conducted in a clean
laboratory environment, 20 ± 2°C and 50 percent relative humidity.
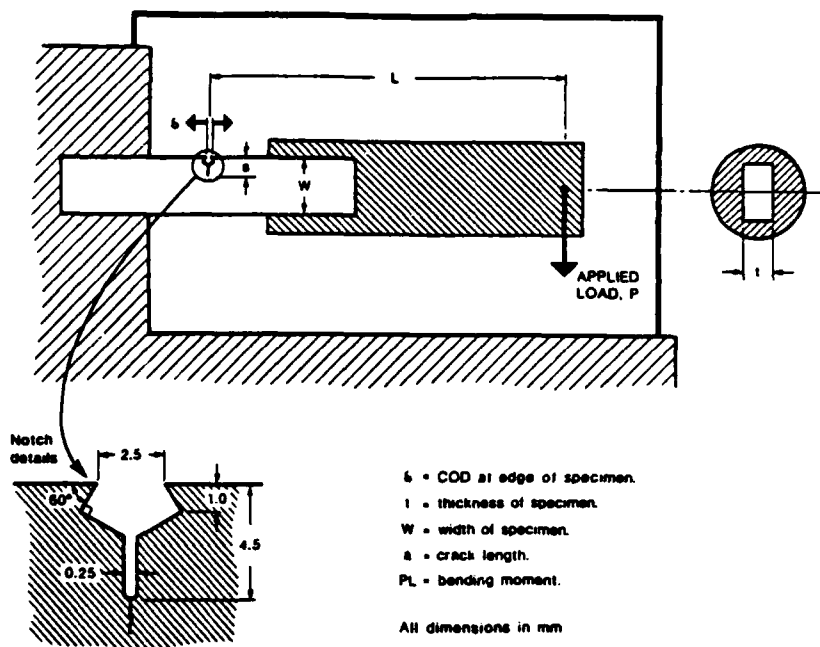

Figure 2.   Specimen details and test setup for stress-corrosion
            cracking studies.

The stress-corrosion testing was performed in constant load cantilever
bending as shown in Figure 2. The relative humidity during the tests was main-
tained at 95 ± 1 percent by using hydrated calcium sulfate salts ($CaSO_4 \cdot H_2O$) in

containers placed inside an environmental chamber. Both the temperature and humidity inside the environmental chamber were monitored continuously during the testing.

The specimen for the tests was immersed in a 3.5 percent NaCl distilled water solution for 1 hour, and following removal, left to dry in laboratory air for 24 hours. The specimen was then installed in the cantilever-bend test set-up, and test loading was commenced after the air inside the test chamber reached 95 percent relative humidity.

Individual specimens were loaded to preselected values. A clip gage of the ASTM type (ref 9) was mounted across the specimen notch and the crack opening displacement, δ, was monitored through a data acquisition system. The system consisted of a 20-channel amplifier receiving the clip gage signal, an analog-to-digital converter, and a printer which was programmed to print and record at preset time intervals.

An inverse form of the relation for δ in terms of a/W given by Tada et al. (ref 10) for pure bending was used to calculate a/W. The Tada et al. relation is

$$\frac{\delta BWE}{PL} = 24(a/W)[0.8 - 1.7(a/W) + 2.4(a/W)^2 + \frac{0.66}{(1-a/W)^2}] \qquad (1)$$

for the range 0 < a/W < 1

where

   B = specimen thickness

   PL = bending moment at the crack plane

   E = Young's modulus

Joyce et al. (ref 11) expressed the above relation in an inverse polynomial form which was further modified (ref 12) for use here

6

$$a/W = 1 - 3.83A - 1.81A^2 + 32.3A^3 - 44.2A^4 - 52.7A^5 \tag{2}$$

where

$$A = 1/[(\delta BWE/PL)^{\frac{1}{2}} + 1]$$

for the range $0.3 < a/W < 1$.

Using the crack length and the applied loads, the stress intensity, K, at the crack tip was evaluated from the expression described by Tada et al. (ref 10)

$$KBW^{3/2}/PL = 6(2 \tan \frac{\pi}{2} \frac{a}{W})^{\frac{1}{2}} \; \frac{(0.923 + 0.199(1-\sin \frac{\pi}{2} \frac{a}{W})^4}{\cos \frac{\pi}{2} \frac{a}{W}} \tag{3}$$

for the range $0 < a/W < 1$.

In this study the δ expression used (Eq. (1)) is for plane-stress conditions. The reason for this is that the δ measurements were at some distance from the crack tip and therefore involve a large portion of the specimen. Plane-strain conditions dominate only very near the crack tip, whereas any displacement measurement away from the tip should be predominantly plane-stress. From this reasoning, the critical values of K (K_{Ic} and K_{Iscc}) are plane-strain values, whereas the δ values are plane-stress. Later, it is shown that a/W values calculated from δ (assuming plane-stress conditions) were in close agreement with those determined directly from fracture surfaces. An analogy can be found in Newman's (ref 13) work on the standard compact specimen. Newman showed that δ measurements for a range of a/W ratios were bounded by the calculated δ values for plane-stress and plane-strain conditions. A closer observation showed that the δ measurements at and above (a/W) = 0.5 were in much closer agreement with the plane-stress calculations than with plane-strain.

7

RESULTS AND DISCUSSION

Strength and Toughness

The complex chemistry and structure of the liquid-phase sintered tungsten alloys can lead to difficulty in understanding the resultant mechanical properties. For example, in Table II there is no significant difference in the as-received composite hardness with significant variations in tungsten particle size, tungsten composition, and matrix phase elements (cf. alloys 95WNiFe, 97WNiFeCuCo, and 90WNiCu). Considering the as-received condition of alloy 90WFeNi, it appears that an increase in hardness and strength can be achieved by a post-sintering mechanical operation such as swaging. This increase in composite hardness is associated with the deformation and resulting hardening of the matrix structure.

Analysis of the tensile test data and Brinell hardness (ref 14) measurements on alloy 95WNiFe was performed in order to obtain a correlation between ultimate tensile strength and hardness. Using the ultimate tensile strength of 901 MPa (92 Kgf/mm^2) and hardness of 283 HB (Kgf/mm^2) for alloy 95WNiFe, the following hardness-to-strength correlation was obtained:

$$\sigma_{uts} = 0.325 \text{ HB} \tag{4}$$

The determination of σ_{uts} for the other three alloys was carried out using the above correlation and their respective hardness values.

The fracture toughness of the alloys was determined using both three-point bend and cantilever-bend tests. The toughness values reported in Table II are average K_{max} values obtained from one of each type of test. Figure 3 shows the results from cantilever-bend tests in terms of applied stress intensity, K_{appl}, as a function of δ. One alloy, 90WFeNi, was found to meet the specimen size requirements for plane-strain fracture toughness (ref 9). For other alloys the

8

fracture toughness values in Table II may be higher than the actual values, perhaps by about 5 percent.

The results show the loss in fracture toughness as the binder content decreases (cf. alloys 97WNiFeCuCo, 95WNiFe, and 90WNiCu); even a post-sintering mechanical treatment did not appear to cause as significant a loss in toughness as that associated with a reduced binder content (cf. alloys 97WNiFeCuCo and 90WFeNi).
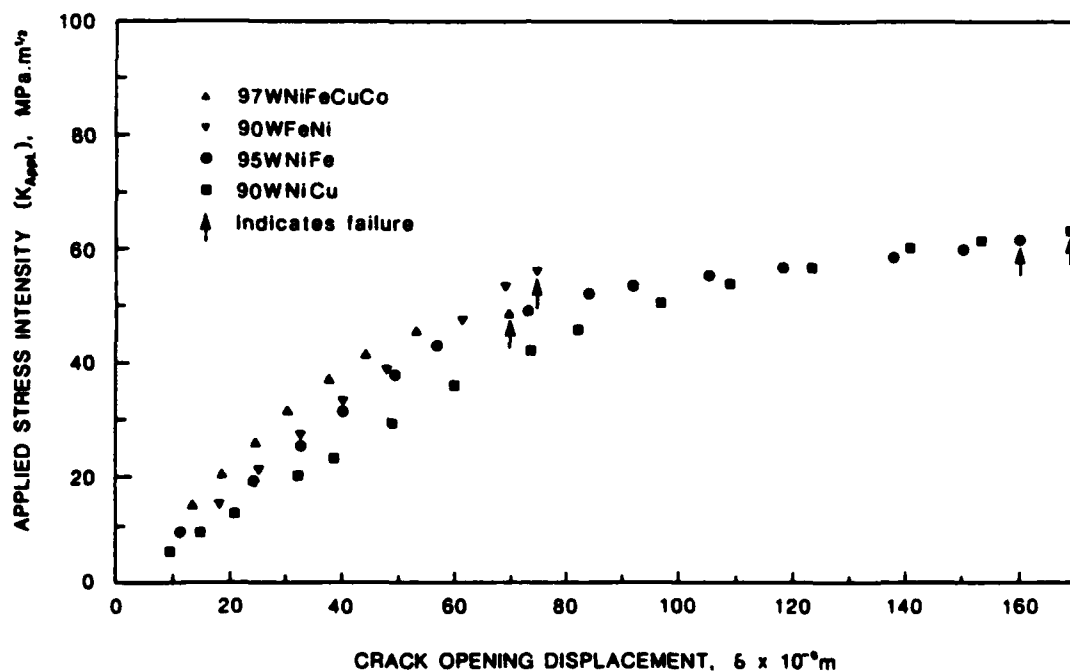
Figure 3. Response of notched alloy bars in cantilever-bend tests.

Fractography

Fractures in Fatigue and Bending Overload

Examination of the fatigue precrack region of the fracture surfaces showed the characteristic fatigue striations in the binder, areas of tungsten-tungsten separation, and areas of tungsten cleavage. Areas of tungsten-binder separation were also seen in alloy 97WNiFeCuCo which had the lowest binder content. Figure 4 depicts the modes of fatigue crack growth as mentioned above.

9

Figure 4. Scanning electron fractographs illustrating modes of failure
under fatigue loading: tungsten particle cleavage (A), fatigue
striations in the binder (B), tungsten-tungsten separation (C),
and tungsten-binder separation (D). (a) Alloy 95WNiFe and (b)
alloy 97WNiFeCuCo.

The fracture surface in the bending overload region for alloys having a 10 and 5 percent binder consisted primarily of binder failure by microvoid coalescence, cleavage of tungsten, and tungsten-tungsten separation. In the case of alloy 97WNiFeCuCo, which had a 3 percent binder, the overload fracture region consisted mainly of tungsten-binder separation, microvoid coalescence in the binder, and tungsten-tungsten separation; cleavage of tungsten particles was negligible. Figure 5 shows the overload region with various modes of failure as mentioned above.

Several investigations (refs 2,15,16) have identified similar failure modes in tungsten alloys. Generally, these studies have showed that tungsten-binder separation, as seen in alloy 97WNiFeCuCo, tends to reduce the ductility of these alloys. The present study shows that tungsten particle cleavage is associated with the presence of two conditions. First, in order to bring about cleavage failure, a certain amount of particle-particle contact seems to be required. Second, the plane of the cleavage crack is typically observed to be at a right angle to the particle-particle contact area. Figures 4a and 5a show examples of these features of the cleavage failure mechanism. Note the extension of the cleavage fracture pattern from one particle to another over the contact boundary. In a situation where the cleavage plane lies approximately in the plane of the contact surface, crack extension occurs by separation at the tungsten-tungsten interface.

Fracture Under Stress-Corrosion

A knowledge of residual manufacturing stresses in these alloy systems is of great importance. If significant residual stresses are present, the long-term structural integrity of components could be affected. One way to observe their presence is to expose the alloys to the test environment free from
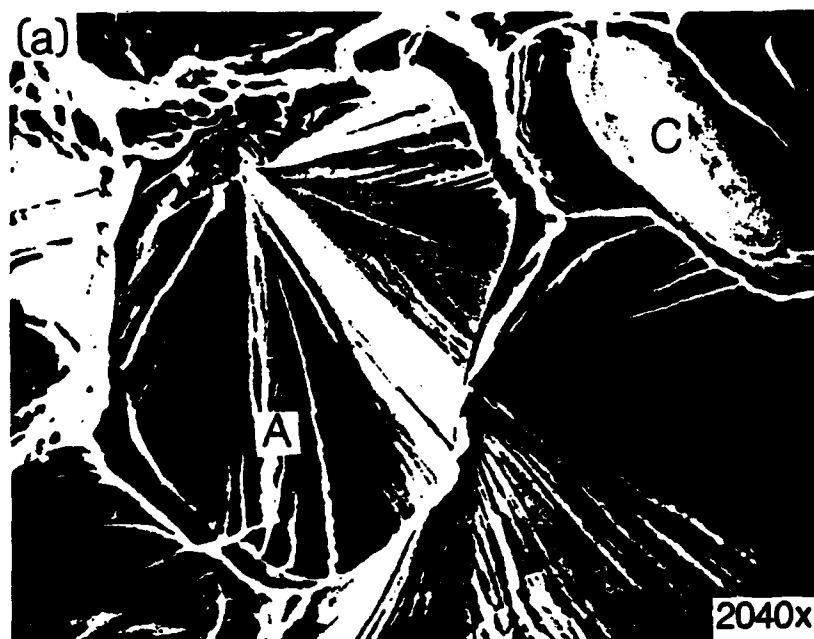
11

Figure 5. Scanning electron fractographs showing the various modes of failure in bending load: tungsten particle cleavage (A), microvoid coalescence in the binder (B), tungsten-tungsten separation (C), and tungsten-binder separation (D). (a) Alloy 90WFeNi and (b) alloy 97WNiFeCuCo.

12

externally applied stresses. In such conditions, cracking may occur if high
enough tensile residual stresses are present in locations exposed to an aggres-
sive environment. Such a study was conducted on 10-mm square polished speci-
mens. After 500 hours of exposure, isolated regions of the binder showed
dissolution which resulted in the formation of a mud-cracklike pattern on the
surface. These regions were numerous in alloy 90WNiCu, while alloy 97WNiFeCuCo,
having the lowest binder content, displayed fewer such regions. Alloys 90WFeNi
and 95WNiFe were also found to be susceptible to such behavior, but to a much
lesser extent. Figure 6 illustrates the regions where the above phenomenon

Figure 6. Scanning electron micrograph showing mud-cracklike pattern in the
binder after the polished specimen of alloy 90WNiCu was immersed
in 3.5 percent NaCl solution and then exposed for 500 hours in
95 percent relative humidity with no external stress.

13

occurred in the test environment. Chung and Duquette (ref 8) made a similar observation in a 90WFeNi alloy and associated it with the presence of a brittle interphase boundary precipitate. The existence of a brittle intermetallic phase in tungsten alloys was also identified previously by other researchers (refs 3,17,18). Optical metallography of sections beneath this product showed the absence of sub-surface cracks, thus ruling out manufacturing residual stresses in the alloys as causing stress-corrosion cracking.

The fracture surface of the specimens which failed by stress-corrosion with the usual sustained external loading displayed cleavage of tungsten particles, tungsten-tungsten particle separation, and microvoid coalescence in the binder. As mentioned before, alloy 97WNiFeCuCo displayed, in addition to the above failure modes, tungsten-binder separation. These failure modes, in combination with dissolution of the isolated regions of the binder, assisted in the overall crack growth. Figure 7 shows the stress-corrosion cracking fracture surfaces with mud-cracklike patterns clearly visible.

Unloading Compliance Method

The concept of using a compliance technique to measure crack extension was first put forth by Irwin (ref 19). Later, Clarke et al. (ref 20) developed this technique and successfully applied it to single specimen crack extension measurement for J-integral fracture toughness testing. The unloading compliance technique was found to be suitable in the present study for a number of reasons. First, the technique overcame the problems of mechanical and electrical drift commonly observed in long-term K_{Iscc} tests. Also, the technique gave measurements averaged over the whole crack front. Finally, the inherent difficulty in direct observation of stress-corrosion crack growth on the specimen surface was removed through the use of unloading compliance.
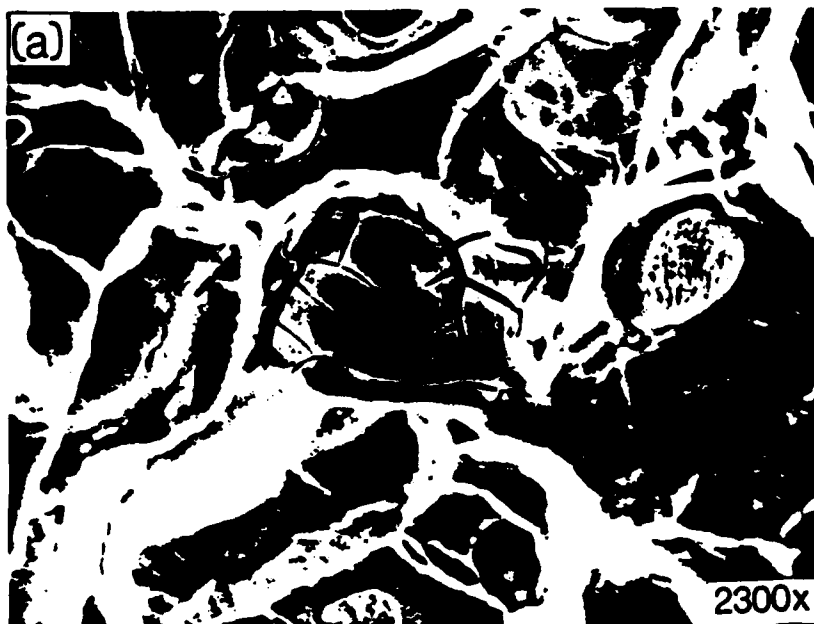
14

Figure 7. Scanning electron micrographs of stress-corrosion cracking fracture surfaces: (a) 90WFeNi and (b) 90WNiCu.

Consider for example, alloy 90WFeNi, which was subjected to an applied
stress intensity of 45.9 MPa $m^{\frac{1}{2}}$ in the environment previously described. Table
III compares the calculated plane-strain and plane-stress a/W values with the
measured values of the fatigue precrack length from the fracture surface. The
maximum difference between the calculated plane-stress values and the measured
a/W values was less than 2 percent. For a similar comparison using plane-strain
conditions, the disagreement widens between the calculated and measured a/W
values, as shown in Table III. This shows that the plane-stress assumption is
more appropriate for an unloading compliance procedure that involves a large
portion of the specimen. In contrast, plane-strain conditions predominate very
near the crack tip so that calculated stress intensities (i.e., K_{appl} and K_{Iscc})
are plane-strain quantities.

TABLE III. COMPARISON OF CALCULATED a/W UNDER PLANE-STRESS AND
PLANE-STRAIN CONDITIONS WITH MEASURED a/W

Calculated a/W		Measured a/W	
Plane-Strain	Plane-Stress	Five-Point Average	Alloy
0.536	0.519	0.509	90WFeNi
0.533	0.517	0.507	90WNiCu
0.522	0.505	0.501	97WNiFeCuCo
0.525	0.508	0.504	95WNiFe

Another set of example results shows that stress-corrosion crack growth was
conveniently monitored using the unloading compliance procedure. Alloy 90WFeNi
was subjected to an initial sustained stress intensity of 45.9 MPa $m^{\frac{1}{2}}$ in the
test environment. Table IV shows the calculated and measured crack growth in
this particular test. As indicated in the footnote, the assumed Young's modulus
was corrected to an effective modulus so that the calculated a/W (determined

using unloading compliance) agreed with the measured a/W (from the fracture surface) at time equals zero. This procedure improves the accuracy of subsequent crack growth calculations. Figure 8 shows a plot of (a/W)* versus time, where the (a/W)* values were calculated using the effective modulus. Due to the difficulty in monitoring fast crack growth in the final stages, the last calculated a/W data point did not occur at the same time as the final failure.

Unloading compliance measurements were used to identify an apparent crack closure phenomenon during some of the K_{Iscc} tests. Typically, general corrosion was occurring and the corrosion products were hindering the normal movement of the notch faces during the partial unloading/reloading exercise. This resulted in an apparent decrease in calculated a/W as a function of time.

TABLE IV. CALCULATED AND MEASURED CRACK LENGTH DATA FOR ALLOY 90WFeNi[†]

| Sustained Load Time Increment | δEBW/M Unloading | a/W | | δE*BW/M Unloading | (a/W)* Calculated Eq. (1) |
		Calculated Eq. (1)	Measured 5-Point Average		
0	42.7	0.519	0.509	40.3	0.509
1	43.8	0.524	-	41.4	0.515
2	46.8	0.536	-	44.2	0.526
3	51.3	0.552	-	48.5	0.542
4	53.7	0.559	-	50.7	0.550
5	64.4	0.590	-	60.9	0.581
6	-	-	0.664	-	-

$E* = E[\dfrac{δEBW/PL \text{ measured}; t=0}{δEBW/PL \text{ calculated}; t=0}]$

[†]Specimen immersed in 3.5 percent NaCl aqueous solution followed by sustained loading in 95 percent relative humidity air; E = 370,000 MPa; effective modulus, E* = 349,500 MPa; failure time = 92 hours, 46 minutes.

17
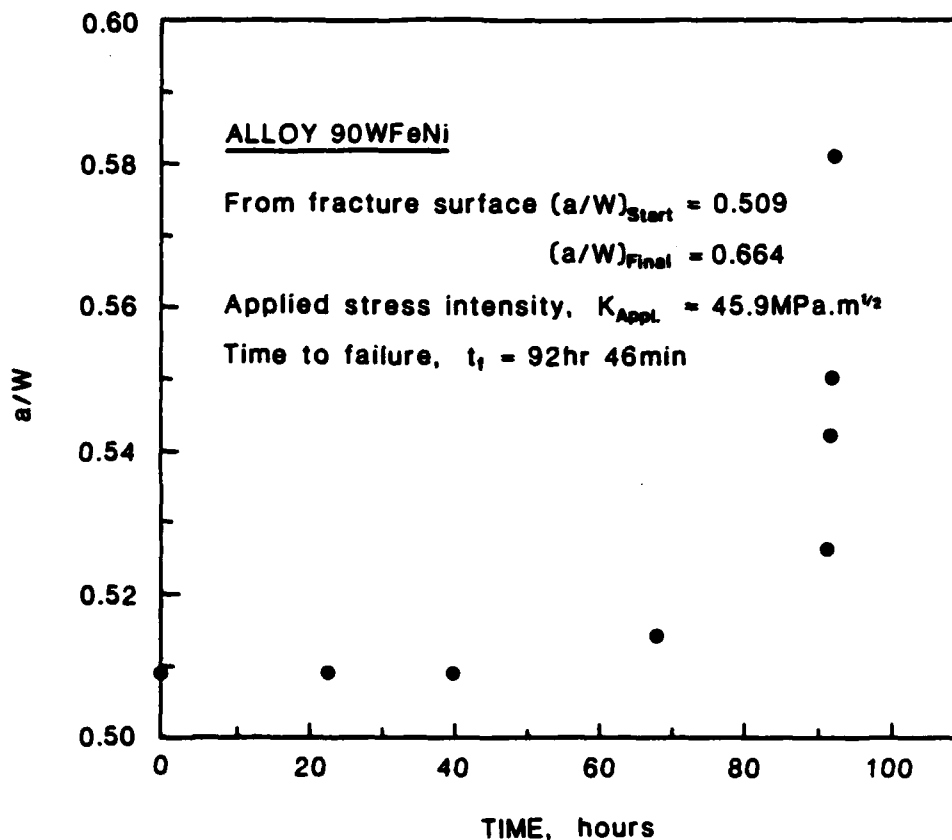
Figure 8. Stress-corrosion crack extension as determined using
the unloading compliance procedure. The data points
correspond to the quantities in Table IV.

Figure 9 illustrates the result corresponding to the crack closure phenome-

non in terms of calculated a/W versus time. The alloy, 90WFeNi, was loaded to a

stress intensity of 40.0 MPa $m^{1/2}$, a value below the alloy's K_{Iscc}. The test was

stopped after 500 hours and the notch area was flushed with distilled water in

an attempt to remove any corrosion products from between the notch faces.

Following this, the specimen was loaded again to the stress intensity level ini-

tially used and an immediate unloading/reloading was performed to determine the

a/W. As shown in Figure 9, the value of a/W recovered to about the value

obtained at the start of the test.
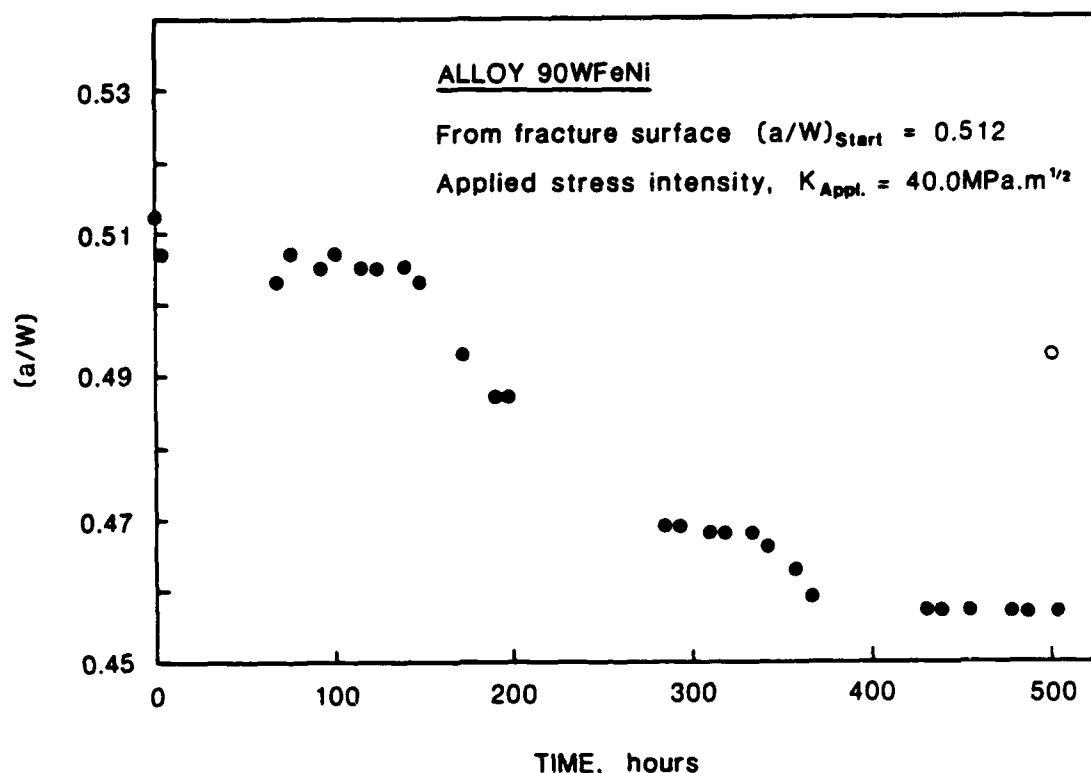
Figure 9. Crack closure phenomenon as observed during stress-corrosion
cracking tests using the unloading compliance techique.
The open circle corresponds to a/W obtained after cleaning
off the corrosion products.

Similar apparent crack length reduction was observed by Joyce et al. (ref

11) working with depleted uranium specimens. In their study, the reduction in

crack length occurred over the first 5 hours of the test and resulted in speci-

men failure. The authors attributed this behavior to the presence of residual

stresses and a plastic zone resulting from fatigue precracking. By contrast, in

the present study, the apparent reduction in a/W was seen for an extended period

in specimens which did not fail, and was due to the accumulation of corrosion

products between the notch faces.

Stress-Corrosion Threshold

The resistance of materials to stress-corrosion cracking is measured in terms of a stress intensity threshold designated as K_{Iscc} below which no crack extension occurs. Two approaches (refs 21,22) have been used extensively in which specimens are loaded to various levels of stress intensities and either the crack velocity, da/dt, or the time to failure, t_f, is measured (see Figure 10).
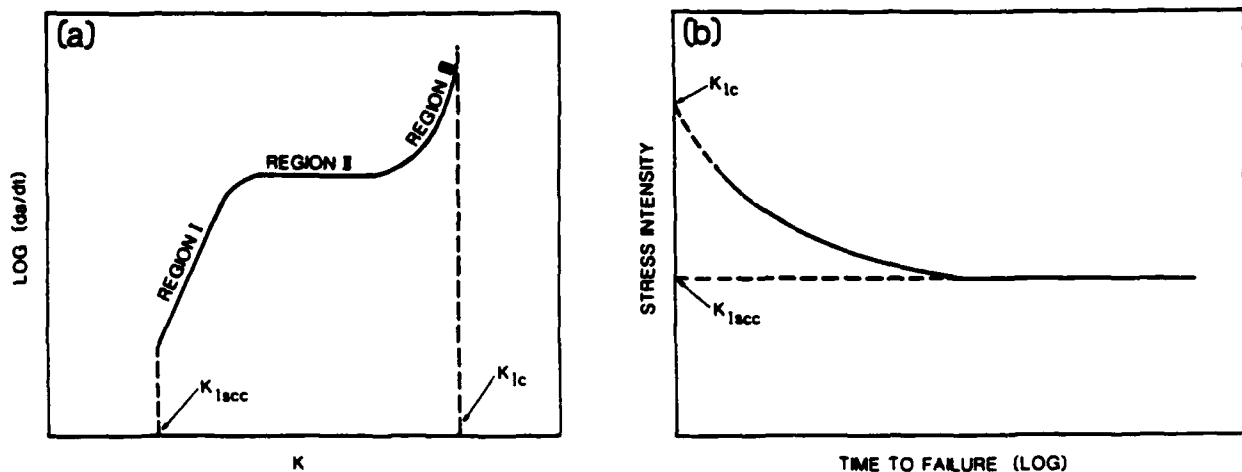
Figure 10. Two approaches in determining K_{Iscc}: (a) da/dt versus K and (b) K versus t_f.

The da/dt versus K approach involves three regions with regions I and III being strongly stress-dependent. The K_{Iscc} is obtained by extrapolating the lower end of region I to the abscissa. However, the measurement of K_{Iscc} using da/dt versus K curve becomes difficult where the material behavior does not show region I. In such a case, the K_{Iscc} can be practically determined from the K versus t_f curve (Figure 10b) by observing at what initial K level no failure occurs after a certain test duration, e.g., 500 hours.

20

In the alloys investigated here, the evidence of stress-corrosion cracking was found in the stress intensity-dependent region III. For this reason the ranking of the alloys according to their resistance to stress-corrosion cracking was accomplished by measuring K_{Iscc} from the K_{appl} versus t_f curve. All the alloys showed susceptibility to stress-corrosion failure in an environment of 3.5 percent NaCl immersion followed by sustained loading in 95 percent relative humidity air.

Figure 11 illustrates the overall results in the form of K_{appl} versus t_f curves. These curves were extrapolated upward to coincide with the respective alloys' fracture toughness, since the toughness is unlikely to be affected by environment in the fraction of a second required for fast failure. The threshold K_{Iscc} for the alloys varied from 32.6 MPa $m^{\frac{1}{2}}$ for alloy 97WNiFeCuCo to 53.6 MPa $m^{\frac{1}{2}}$ for alloy 95WNiFe. The K_{Iscc} was not much different for the two 10 percent binder alloys, although the 90WNiCu alloy displayed a larger drop from its fracture toughness value to its K_{Iscc} value.

One of the alloys tested here, 97WNiFeCuCo, had the same composition as an alloy tested by Chung and Duquette (ref 8). Also, a similar environment was used, albeit in a different way. The earlier K_{Iscc} results were quite different from those observed in the present study. The earlier work found no evidence of stress-corrosion cracking, whereas in the present work, $K_{Iscc} = 32.6$ MPa $m^{\frac{1}{2}}$. This difference in K_{Iscc} behavior may be due to the difference in environment, exposure time, and type of loading. The bolt-loading used in the earlier study involved a value of K_{appl} at about the level of K_{Ic}, which could cause extreme crack tip plasticity therefore preventing or delaying stress-corrosion cracking. The lower values in cantilever loading, which established the K_{Iscc} in the present study, precluded any such overload.

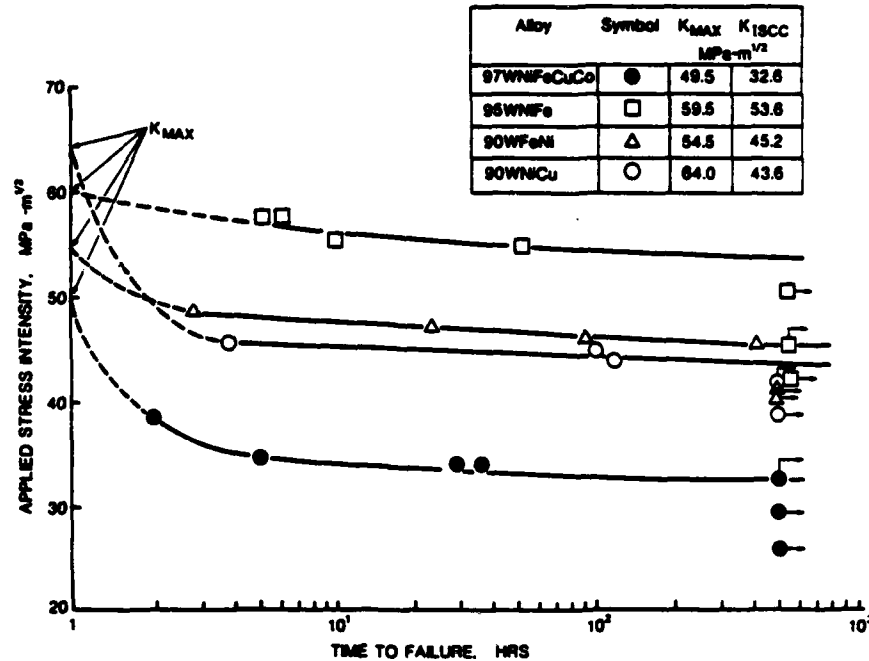| Alloy	Symbol	K_{MAX}	K_{ISCC}
		MPa-m$^{1/2}$	
97WNiFeCuCo	●	49.5	32.6
95WNiFe	□	59.5	53.6
90WFeNi	△	54.5	45.2
90WNiCu	○	64.0	43.6

Figure 11. Stress-corrosion cracking of W alloys in terms of applied
stress intensity as a function of time to failure.

An important practical implication of the present study is the following.
When tungsten alloy components are subjected to significant levels of sustained
tensile stress, including residual manufacturing stresses, storage should
preclude chloride-containing environments, specially marine, in order to extend
their shelf life and maintain their structural integrity in application.

CONCLUSIONS

The following conclusions were drawn from this study:

1. All the alloys investigated displayed susceptibility to stress-
corrosion cracking in an environment of 3.5 percent NaCl immersion followed by
sustained loading in 95 percent relative humidity air. Alloy 95WNiFe showed the
least susceptibility and the narrowest range for stress-corrosion cracking.

22

2. Fracture mechanics provided a quantitative assessment and ranking of the resistance to stress-corrosion cracking of the various alloys.

3. A variety of failure modes were observed in the alloy systems. The environment caused localized dissolution of binder regions and was responsible for crack growth under external sustained loads.

4. An unloading compliance procedure similar to that applied in J-integral testing gave accurate measurements of stress-corrosion crack growth.

5. A crack closure phenomenon was identified using the unloading compliance procedure and attributed to the accumulation of corrosion products between the crack faces following certain exposure times to the environment.

REFERENCES

1. J. W. O'Neil and P. N. Salyer, "Effect of Tungsten Composition on the Mechanical Properties on the W-Ni-Fe Heavy Alloy," Massachusetts Institute of Technology, ASRL TR 132-2, Air Force Office of Scientific Research, AFOSR 66-1670, December 1965.

2. K. S. Churn and R. M. German, "Fracture Behavior of W-Ni-Fe Heavy Alloys," Metall. Trans., Vol. 15A, No. 2, February 1984, pp. 331-338.

3. D. V. Edmonds and P. N. Jones, "Interfacial Embrittlement on Liquid-Phase Sintered Tungsten Heavy Alloys," Metall. Trans., Vol. 10A, No. 3, March 1979, pp. 289-295.

4. T. K. Kang, E. T. Henig, W. A. Kaysser, and G. Petzow, in: Modern Developments in Powder Metallurgy, (H. H. Hausner, H. W. Antes, and G. D. Smith, eds.), Metal Powder Industries, Princeton, NJ, Vol. 14, 1981, pp. 189-203.

5. K. S. Churn and D. N. Yoon, "Pore Formation and Its Effect on Mechanical Properties in W-Ni-Fe Heavy Alloy," Powder Metall., Vol. 22, 1979, pp. 175-178.

6. B. C. Muddle and D. V. Edmonds, "Interfacial Segregation and Embrittlement in Liquid-Phase Sintered Tungsten Alloys," Philos. Trans. R. Soc. London., Vol. A295, No. 1413, 1980, p. 129.

7. R. M. German and J. E. Hanafee, "Processing Effects on Toughness for Liquid Phase Sintered W-Ni-Fe," Processing of Metal and Ceramic Powders, (R. M. German and K. W. Lay, eds.), The Metallurgical Society, AIME, Warrendale, PA, 1982, pp. 267-282.

8. J. G. Chung and D. J. Duquette, "Stress Corrosion Cracking Behavior of Tungsten Heavy Alloys," ARDC Contractor Report ARLCB-CR-84034, Rensselaer Polytechnic Institute, Troy, NY, October 1984.

9. "Standard Test Method for Plane-Strain Fracture Toughness of Metallic Materials, ASTM E-399," 1987 Annual Book of ASTM Standards, Vol. 03.01, ASTM, Philadelphia, PA, 1987, pp. 680-715.

10. H. Tada, P. C. Paris, and G. R. Irwin, The Stress Analysis of Cracks Handbook, Del Research Corporation, Hellertown, PA, 1973.

11 J. A. Joyce, D. F. Hasson, and C. R. Crowe, "Computer Data Acquisition Monitoring of the Stress Corrosion Cracking of Depleted Uranium Cantilever Beam Specimens," J. of Testing and Evaluation, Vol. 8, November 1980, pp. 293-300.

12. J. H. Underwood, I. A. Burch, and M. Z. Shah Khan, Materials Research Laboratory Report, to be published.

13. J. C. Newman, Jr., "Stress Analysis of the Compact Specimen Including the Effects of Pin Loading," _Fracture Analysis_, ASTM STP 560, American Society for Testing and Materials, Philadelphia, PA, 1974, pp. 105-151.

14. "Standard Test Method for Brinell Hardness of Metallic Materials, ASTM E-10," _1987 Annual Book of ASTM Standards_, Vol. 03.01, ASTM, Philadelphia, PA, 1987, pp. 236-246.

15. R. H. Krock, "Some Comparisons Between Fiber-Reinforced and Continuous Materials," _J. Mater._, Vol. 1, No. 2, June 1966, pp. 278-292.

16. E. G. Zukas, "Coating Tungsten Composites for Improved Low Temperature Ductility," _Metall. Trans._, Vol. 7B, No. 1, March 1976, pp. 49-54.

17. B. C. Muddle, "Interphase Boundary Precipitation in Liquid Phase Sintered W-Ni-Fe and W-Ni-Cu Alloys," _Metall. Trans._, Vol. 15A, 1984, pp. 1089-1098.

18. R. L. Woodward, N. J. Baldwin, I. Burch, and B. J. Baxter, "Effect of Strain Rate on the Flow Stress of Three Liquid Phase Sintered Tungsten Alloys," _Metall. Trans._, Vol. 16A, November 1985, pp. 2031-2037.

19. G. R. Irwin, "Structural Aspects of Brittle Fracture," _Applied Materials Research_, Vol. 3, No. 2, April 1964, pp. 65-81.

20. G. A. Clarke, W. R. Andrews, P. C. Paris, and D. W. Schmidt, "Single Specimen Tests for J_{Ic} Determination," _Mechanics of Crack Growth_, ASTM STP 590, American Society for Testing and Materials, Philadelphia, PA, 1976, pp. 27-42.

21. B. F. Brown and C. D. Beachem, "A Study of the Stress Factor in Corrosion Cracking by Use of the Precracked Cantilever-Beam Specimen," _Corrosion Science_, Vol. 5, No. 11, November 1965, pp. 745-750.

22. M. O. Speidel and M. V. Hyatt, _Advances in Corrosion Science and Technology_, Vol. 2, Plenum Press, New York, 1972, pp. 115-335.

TECHNICAL REPORT INTERNAL DISTRIBUTION LIST

	NO. OF COPIES
CHIEF, DEVELOPMENT ENGINEERING BRANCH	
ATTN: SMCAR-CCB-D	1
-DA	1
-DC	1
-DM	1
-DP	1
-DR	1
-DS (SYSTEMS)	1
CHIEF, ENGINEERING SUPPORT BRANCH	
ATTN: SMCAR-CCB-S	1
-SE	1
CHIEF, RESEARCH BRANCH	
ATTN: SMCAR-CCB-R	2
-RA	1
-RM	1
-RP	1
-RT	1
TECHNICAL LIBRARY	5
ATTN: SMCAR-CCB-TL	
TECHNICAL PUBLICATIONS & EDITING UNIT	3
ATTN: SMCAR-CCB-TL	
DIRECTOR, OPERATIONS DIRECTORATE	1
ATTN: SMCWV-OD	
DIRECTOR, PROCUREMENT DIRECTORATE	1
ATTN: SMCWV-PP	
DIRECTOR, PRODUCT ASSURANCE DIRECTORATE	1
ATTN: SMCWV-QA	

NOTE: PLEASE NOTIFY DIRECTOR, BENET LABORATORIES, ATTN: SMCAR-CCB-TL, OF ANY ADDRESS CHANGES.

TECHNICAL REPORT EXTERNAL DISTRIBUTION LIST

	NO. OF COPIES		NO. OF COPIES

ASST SEC OF THE ARMY
RESEARCH AND DEVELOPMENT
ATTN: DEPT FOR SCI AND TECH   1
THE PENTAGON
WASHINGTON, D.C. 20310-0103

ADMINISTRATOR
DEFENSE TECHNICAL INFO CENTER
ATTN: DTIC-FDAC   12
CAMERON STATION
ALEXANDRIA, VA 22304-6145

COMMANDER
US ARMY ARDEC
ATTN: SMCAR-AEE   1
     SMCAR-AES, BLDG. 321   1
     SMCAR-AET-O, BLDG. 351N   1
     SMCAR-CC   1
     SMCAR-CCP-A   1
     SMCAR-FSA   1
     SMCAR-FSM-E   1
     SMCAR-FSS-D, BLDG. 94   1
     SMCAR-IMI-I (STINFO) BLDG. 59   2
PICATINNY ARSENAL, NJ 07806-5000

DIRECTOR
US ARMY BALLISTIC RESEARCH LABORATORY
ATTN: SLCBR-DD-T, BLDG. 305   1
ABERDEEN PROVING GROUND, MD 21005-5066

DIRECTOR
US ARMY MATERIEL SYSTEMS ANALYSIS ACTV
ATTN: AMXSY-MP   1
ABERDEEN PROVING GROUND, MD 21005-5071

COMMANDER
HQ, AMCCOM
ATTN: AMSMC-IMP-L   1
ROCK ISLAND, IL 61299-6000

COMMANDER
ROCK ISLAND ARSENAL
ATTN: SMCRI-ENM   1
ROCK ISLAND, IL 61299-5000

DIRECTOR
US ARMY INDUSTRIAL BASE ENGR ACTV
ATTN: AMXIB-P   1
ROCK ISLAND, IL 61299-7260

COMMANDER
US ARMY TANK-AUTMV R&D COMMAND
ATTN: AMSTA-DDL (TECH LIB)   1
WARREN, MI 48397-5000

COMMANDER
US MILITARY ACADEMY   1
ATTN: DEPARTMENT OF MECHANICS
WEST POINT, NY 10996-1792

US ARMY MISSILE COMMAND
REDSTONE SCIENTIFIC INFO CTR   2
ATTN: DOCUMENTS SECT, BLDG. 4484
REDSTONE ARSENAL, AL 35898-5241

COMMANDER
US ARMY FGN SCIENCE AND TECH CTR
ATTN: DRXST-SD   1
220 7TH STREET, N.E.
CHARLOTTESVILLE, VA 22901

COMMANDER
US ARMY LABCOM
MATERIALS TECHNOLOGY LAB
ATTN: SLCMT-IML (TECH LIB)   2
WATERTOWN, MA 02172-0001

NOTE: PLEASE NOTIFY COMMANDER, ARMAMENT RESEARCH, DEVELOPMENT, AND ENGINEERING
      CENTER, US ARMY AMCCOM, ATTN: BENET LABORATORIES, SMCAR-CCB-TL,
      WATERVLIET, NY 12189-4050, OF ANY ADDRESS CHANGES.

	NO. OF COPIES		NO. OF COPIES
COMMANDER US ARMY LABCOM, ISA ATTN: SLCIS-IM-TL 2800 POWDER MILL ROAD ADELPHI, MD 20783-1145	1	COMMANDER AIR FORCE ARMAMENT LABORATORY ATTN: AFATL/MN EGLIN AFB, FL 32542-5434	1
COMMANDER US ARMY RESEARCH OFFICE ATTN: CHIEF, IPO P.O. BOX 12211 RESEARCH TRIANGLE PARK, NC 27709-2211	1	COMMANDER AIR FORCE ARMAMENT LABORATORY ATTN: AFATL/MNF EGLIN AFB, FL 32542-5434	1
DIRECTOR US NAVAL RESEARCH LAB ATTN: MATERIALS SCI & TECH DIVISION CODE 26-27 (DOC LIB) WASHINGTON, D.C. 20375	1 1	METALS AND CERAMICS INFO CTR BATTELLE COLUMBUS DIVISION 505 KING AVENUE COLUMBUS, OH 43201-2693	1

NOTE: PLEASE NOTIFY COMMANDER, ARMAMENT RESEARCH, DEVELOPMENT, AND ENGINEERING
CENTER, US ARMY AMCCOM, ATTN: BENET LABORATORIES, SMCAR-CCB-TL,
WATERVLIET, NY 12189-4050, OF ANY ADDRESS CHANGES.

SUPPLEMENTARY

INFORMATION

5 April 1989

ERRATA SHEET
(Change Notice)

Cl TO: TECHNICAL REPORT ARCCB-TR-88039

STRESS-CORROSION CRACKING OF
LIQUID-PHASE SINTERED TUNGSTEN ALLOYS

by

M. Z. Shah Khan
J. H. Underwood
I. A. Burch

Please remove the Report Documentation Page
(DD Form 1473) and page iii from above publi-
cation and insert new pages enclosed. Changes
have been made in Blocks 14 and 18 of the
Report Documentation Page, and an additional
acknowledgement has been included on page iii.

US ARMY ARMAMENT RESEARCH, DEVELOPMENT,
AND ENGINEERING CENTER
CLOSE COMBAT ARMAMENTS CENTER
BENET LABORATORIES
WATERVLIET, N.Y. 12189-4050

REPORT DOCUMENTATION PAGE		READ INSTRUCTIONS BEFORE COMPLETING FORM
1. REPORT NUMBER ARCCB-TR-88039	2. GOVT ACCESSION NO.	3. RECIPIENT'S CATALOG NUMBER
4. TITLE (and Subtitle) STRESS-CORROSION CRACKING OF LIQUID-PHASE SINTERED TUNGSTEN ALLOYS		5. TYPE OF REPORT & PERIOD COVERED Final
		6. PERFORMING ORG. REPORT NUMBER
7. AUTHOR(s) M. Z. Shah Khan, J. H. Underwood, and I. A. Burch (See Reverse)		8. CONTRACT OR GRANT NUMBER(s)
9. PERFORMING ORGANIZATION NAME AND ADDRESS US Army ARDEC Benet Laboratories, SMCAR-CCB-TL Watervliet, NY 12189-4050		10. PROGRAM ELEMENT, PROJECT, TASK AREA & WORK UNIT NUMBERS AMCMS No. 6126.23.1BL0.0 PRON No. 1A82ZJWLNMSC
11. CONTROLLING OFFICE NAME AND ADDRESS US Army ARDEC Close Combat Armaments Center Picatinny Arsenal, NJ 07806-5000		12. REPORT DATE October 1988
		13. NUMBER OF PAGES 28
14. MONITORING AGENCY NAME & ADDRESS(if different from Controlling Office) Materials Research Laboratories Defence Science and Technology Organisation P.O. Box 50, Ascot Vale Victoria, 3032, Australia		15. SECURITY CLASS. (of this report) UNCLASSIFIED
		15a. DECLASSIFICATION/DOWNGRADING SCHEDULE

16. DISTRIBUTION STATEMENT (of this Report)

Approved for public release; distribution unlimited.

17. DISTRIBUTION STATEMENT (of the abstract entered in Block 20, if different from Report)

18. SUPPLEMENTARY NOTES

Work performed at Materials Research Laboratories, Australia.
Presented at the Seventh International Conference on Fracture,
University of Houston, Houston, TX, March 1989.
Published in Proceedings of the Conference.

19. KEY WORDS (Continue on reverse side if necessary and identify by block number)

Stress-Corrosion Cracking	Kinetic Energy Penetration
Liquid-Phase Tungsten	Fracture Mechanics
Unloading Compliance	Crack Closure

20. ABSTRACT (Continue on reverse side if necessary and identify by block number)

This study addresses the stress-corrosion cracking susceptibility of liquid-phase sintered tungsten alloys during long-term storage. These alloys are used for kinetic energy penetrators in military applications and it is essential that the structural integrity of the penetrator is not diminished due to the combined action of the chemical environment and the residual manufacturing stresses.

(CONT'D ON REVERSE)

DD FORM 1473 1 JAN 73 EDITION OF 1 NOV 65 IS OBSOLETE

7. AUTHORS (CONT'D)

M. Z. Shah Khan and I. A. Burch
Materials Research Laboratories
Defence Science and Technology Organisation
P.O. Box 50
Ascot Vale, Victoria, 3032
Australia

20. ABSTRACT (CONT'D)

This report describes test methods used for assessing the resistance to stress-corrosion cracking in terms of the stress intensity parameter, K_{Iscc}. The alloys were obtained from different sources and had up to 10 weight percent additions of selected combinations of nickel (Ni), iron (Fe), copper (Cu), and cobalt (Co), and different process variables. Cantilever-bend specimens were used and the test environment was an immersion in 3.5 percent sodium chloride (NaCl) aqueous solution followed by sustained loading in 95 percent relative humidity air.

The findings of this study were as follows: (1) Fracture mechanics was shown to give a good assessment and ranking of the resistance to stress-corrosion cracking of the various alloys. (2) Evidence of stress-corrosion cracking was found in the region controlled by the stress intensity factor, generally designated as region III. (3) An unloading compliance procedure similar to that applied in J-integral testing was shown to give accurate measurements of stress-corrosion crack growth. (4) A crack closure phenomenon was identified using the unloading compliance procedure and attributed to the accumulation of corrosion products between the crack faces following certain exposure times to the environment.

ACKNOWLEDGEMENTS